ELSEVIER

Microporous and Mesoporous Materials 34 (2000) 171–179

MICROPOROUS AND MESOPOROUS MATERIALS

www.elsevier.nl/locate/micromeso

Microporous texture of activated carbon fibres prepared from Nomex aramid fibres

M.C. Blanco López, A. Martínez-Alonso, J.M.D. Tascón *

Instituto Nacional del Carbón, CSIC, Apartado 73, 33080 Oviedo, Spain

Received 3 March 1999; received in revised form 9 August 1999; accepted for publication 17 August 1999

Abstract

Nomex [poly (*m*-phenylene isophthalamide)] was used as a feedstock for the preparation of activated carbon fibres (ACFs). For this purpose, pyrolysis under inert atmosphere (Ar) was followed by activation with CO_2. Two different series of ACFs were prepared by changing the pyrolysis (1123 or 1173 K) and activation temperatures (50 K below pyrolysis). The resulting ACFs were characterised by N_2 (77 K) and CO_2 (273 K) adsorption. The surface area and pore volume increase progressively upon activation: no maxima were found over the burn-off range studied (0–74%). ACFs prepared from Nomex are microporous and exhibit more uniform and narrower porosity than those prepared from Kevlar flock under equivalent conditions. It is believed that these materials could constitute a suitable precursor for carbon molecular sieves.

Keywords: Activated carbon fibres; Carbon dioxide adsorption; Microporosity; Nitrogen adsorption; Nomex

1. Introduction

The preparation of activated carbons has attracted a great deal of attention in recent years because of their numerous applications, which derive from their porous structure [1,2]. The precursors are non-graphitisable carbons, obtained from vegetable matter (wood, nutshells, etc.), non-fusing coals (anthracite or sub-bituminous coals), or synthetic materials (mainly polymers). Activated carbon fibres (ACFs) offer some advantages regarding conventional activated carbons, i.e. higher adsorption rates and capacity.

Feedstock materials for ACFs are usually of low crystallinity, such as viscose rayon, polyacrylonitrile, or coal tar pitch [3]. Alternatively, aramid fibres have also been proposed as high crystallinity precursors, and some studies on N_2 and H_2O adsorption on ACFs produced from woven Kevlar [3,4] and Nomex [5] activated in steam and CO_2 have been reported. Stoeckli et al. [6] have studied the microstructure created by steam and CO_2 activation of Kevlar and Nomex T-455 chars, by using CH_2Cl_2 adsorption and immersion calorimetry. ACFs with a narrow distribution of micropores and, therefore, suitable for the development of molecular sieves, have been successfully prepared by CO_2 activation of a low-price feedstock material such as Kevlar pulp [7].

The narrow microporosity found in ACFs is due to transformations in the material during pyrolysis and subsequent gasification. The thermal degradation of aramid fibres, and in particular that of the two isomers Nomex [poly (*m*-phenylene

* Corresponding author. Tel.: +34-98-528-08-00; fax: +34-98-529-76-62.

E-mail address: tascon@incar.csic.es (J.M.D. Tascón)

1387-1811/00/$ - see front matter
PII: S1387-1811(99)00171-7

isophthalamide)] and Kevlar [poly (*p*-phenylene terephthalamide)], has been studied in detail [8–11]. The differences in thermal behaviour could result in differences in texture development by both isomers.

A number of variables, such as the crystallinity of the starting material and the temperature of pyrolysis and activation, can modify the texture of the char. Yoon et al. [12] have also shown that the carbon yield of Kevlar and Nomex can be increased by carrying out their pyrolysis in various separate stages with isothermal heating at three intermediate temperatures.

In this study, Nomex was used as a precursor of ACFs obtained by CO_2 activation. Two different pyrolysis temperatures were tried (1173 and 1123 K), and the gasification was carried out at 50 K below the pyrolysis temperature. The results are compared with those previously obtained with Kevlar pulp under similar conditions.

2. Experimental

The starting material was crystalline Nomex *tow* 2.2, with an initial humidity of 8.0 wt%. Its elemental analysis, reported as weight percentages on a dry basis, gave: 71.2% C, 3.9% H, 9.7% N, 15.6% O. Elemental analysis was carried out in a LECO CHNS-932 Microanalysis apparatus (with a LECO VTF-900 accessory for oxygen).

Pyrolysis was carried out in a vertical quartz reactor, in which 5–6 g of the precursor were introduced. Temperature was programmed to increase at a rate of 4 K min^{-1} up to 1123 or 1173 K, under Ar flow (50 cm^3 min^{-1}). The temperature was then decreased to 50 K below the pyrolysis temperature, and the flowing gas was then changed to CO_2 (40 cm^3 min^{-1}). The activation was carried out at different time intervals, to achieve different degrees of burn off (BO).

The gases used had a purity of 99.999% (Ar, N_2) and 99.98% (CO_2). Adsorption isotherms were obtained with a NOVA 1200 (Quantachrome) automatic adsorption apparatus. Prior to the measurements, the samples were degassed at 523 K overnight. A carbon black (Spheron 6) was used as standard for the α_S-method. X-ray powder diffractograms were recorded with a Siemens D5000 diffractometer using Cu Kα radiation (λ = 0.154 06 nm) at a step size of 0.01°.

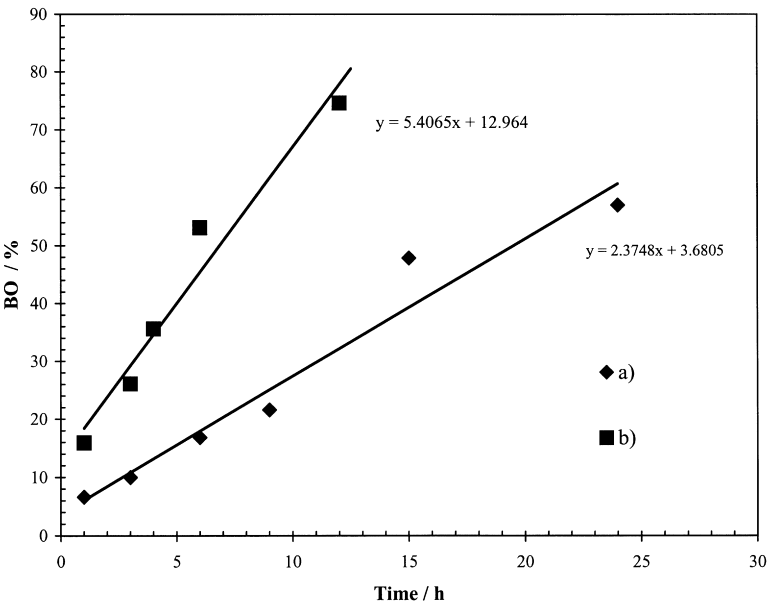

Fig. 1. BO of carbonized Nomex in CO_2 as a function of time at two different pyrolysis and activation conditions: (a) pyrolysis at 1123 K and activation at 1073 K; (b) pyrolysis at 1173 K and activation at 1123 K.

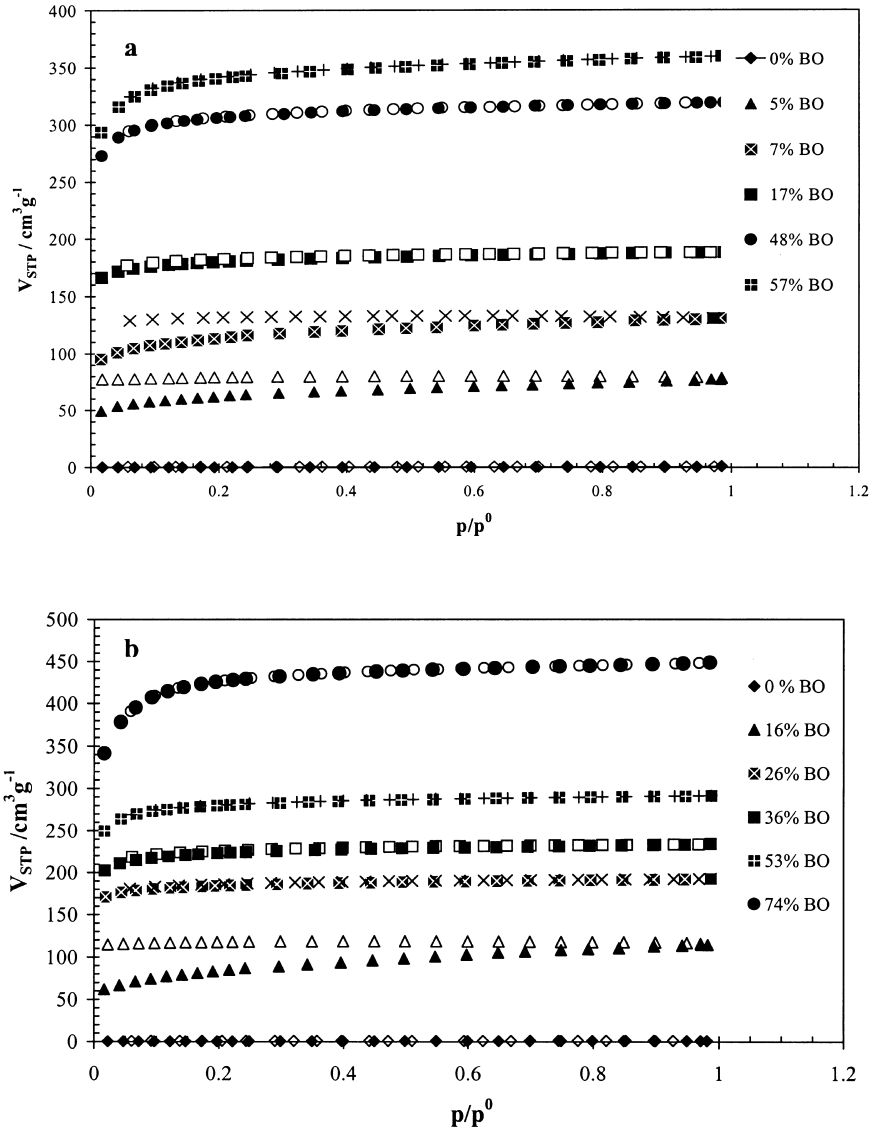

Fig. 2. Adsorption–desorption isotherms of N_2 at 77 K on ACFs prepared by (a) pyrolysis at 1123 K and activation at 1073 K and (b) pyrolysis at 1173 K and activation at 1123 K: full symbols, adsorption; empty symbols, desorption.

3. Results

3.1. Reactivity

Fig. 1 shows the change of BO of carbonised Nomex as a function of the time of CO_2 activation for the two series of samples tested. The data were fitted to a straight line, and the slope was higher for the series prepared at higher temperature (pyrolysis at 1173 K and gasification at 1123 K).

3.2. N_2 adsorption isotherms

The starting material is a non-porous fibre, with $S_{BET} = 0.14\ m^2\ g^{-1}$. After pyrolysis, S_{BET} increased to $0.7\ m^2\ g^{-1}$ (1123 K), and to

1.2 $m^2 g^{-1}$ (1173 K). Fig. 2(a) shows the N_2 adsorption isotherms on chars obtained at several degrees of activation (BO) for the series of samples pyrolysed at 1123 K and activated at 1073 K. Fig. 2(b) shows the series prepared by pyrolysis at 1173 K and activation at 1123 K. All isotherms are of Type I in the BDDT classification, except that of the pyrolysed material, which was of Type II. The presence of a plateau at relative pressures <0.1 indicates microporosity. The angle of the isotherms opens slightly at high BO (60%), indicating that the pores become slightly wider upon activation. However, the increase of the slope is very low, suggesting that the external surface does not change much with the activation degree. It is clear, too, that the capacity of adsorption increases progressively with the BO.

Table 1 shows the textural parameters calculated from N_2 adsorption at 77 K, including parameters deduced from an application of the α_S-method, which gives plots of the type shown in Fig. 3. In this method the adsorbed amount is plotted against the normalised adsorption $\alpha_S = n/n_{0.4}$ (n, uptake at each point; $n_{0.4}$, uptake at a relative pressure of 0.4) obtained from an isotherm measured on a reference non-porous solid (Spheron 6 carbon black was used in this work). As with the t-method, if there is microporosity in a solid the uptake will be enhanced in the low relative pressure region of the isotherms and the curve will be broken into several straight lines (see Fig. 3). The high-pressure branch, when extrapolated to the adsorption axis, gives a positive intercept that is equivalent to the micropore volume ($V_{\mu p}$ in Table 1).

Table 1 also gives the volume adsorbed at high relative pressure (0.95), which can be considered as the total pore volume V_p. The BET surface area S_{BET} and total porosity V_p increase with the degree of activation over the entire BO range studied.

3.2. CO_2 adsorption isotherms

Fig. 4 shows the adsorption isotherms for the ACFs obtained after pyrolysis at 1173 K and activation at 1123 K. Table 2 shows the textural parameters obtained from an application of the DRK equation to CO_2 adsorption, which gives the plots shown in Fig. 5. The micropore volume $V_{\mu p}$ obtained from the DRK equation increases from 0.04 $cm^3 g^{-1}$ in the starting material to 0.19 $cm^3 g^{-1}$ for the material pyrolysed at 1123 K,

Table 1
Textural parameters deduced from N_2 adsorption at 77 K

BO (wt%)	S_{BET} ($m^2 g^{-1}$)	V_p ($cm^3 g^{-1}$)	V_p (%)		α_S-method		
			$V_{p/p^0=0.02}$	$V_{p/p^0=0.2}$	S_{ext} ($m^2 g^{-1}$)	$V_{\mu p}$ ($cm^3 g^{-1}$)	$V_{u\mu p}$ ($cm^3 g^{-1}$) ($\alpha<1$)
Pyrolysis at 1123 K and activation at 1073 K							
0	0.7	0.001	7.4	32.2	0.7	–	–
5	212	0.12	64.0	79.3	4.0	0.11	0.05
7	384	0.20	74.0	87.0	3.5	0.19	0.11
10	428	0.22	69.4	90.15	4.5	0.22	0.12
17	662	0.29	88.6	95.4	4.0	0.29	0.25
48	1128	0.49	86.3	95.6	3.7	0.49	0.43
57	1260	0.55	83.0	94.6	4.8	0.55	0.46
Pyrolysis at 1173 K and activation at 1123 K							
0	1.2	0.002	19.2	24.9	–	–	–
16	291	0.18	53.5	70.0	4.7	0.17	0.07
26	659	0.30	89.2	94.4	2.5	0.29	0.25
36	802	0.36	86.5	95.3	2.8	0.35	0.30
53	1035	0.45	86.1	95.6	1.3	0.45	0.37
74	1545	0.69	77.2	94.9	5.1	0.68	0.58

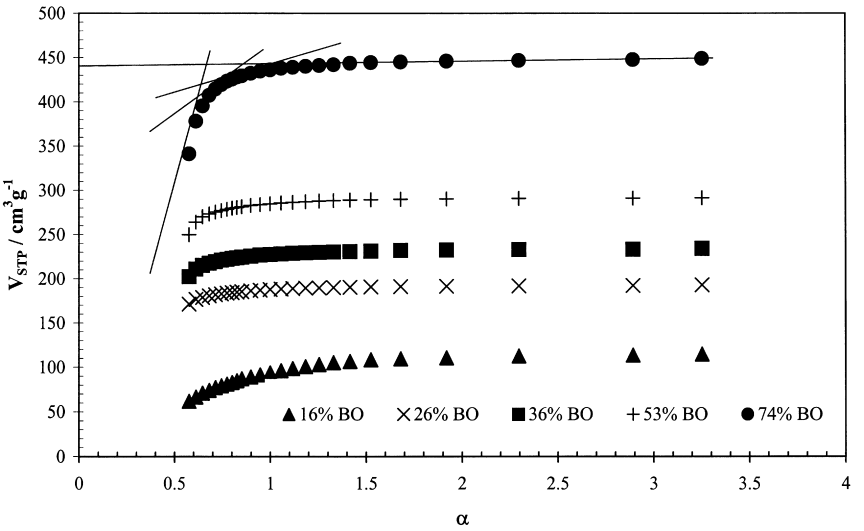

Fig. 3. The α_S-plots for N_2 adsorption isotherms of ACFs prepared by pyrolysis at 1173 K and activation at 1123 K.

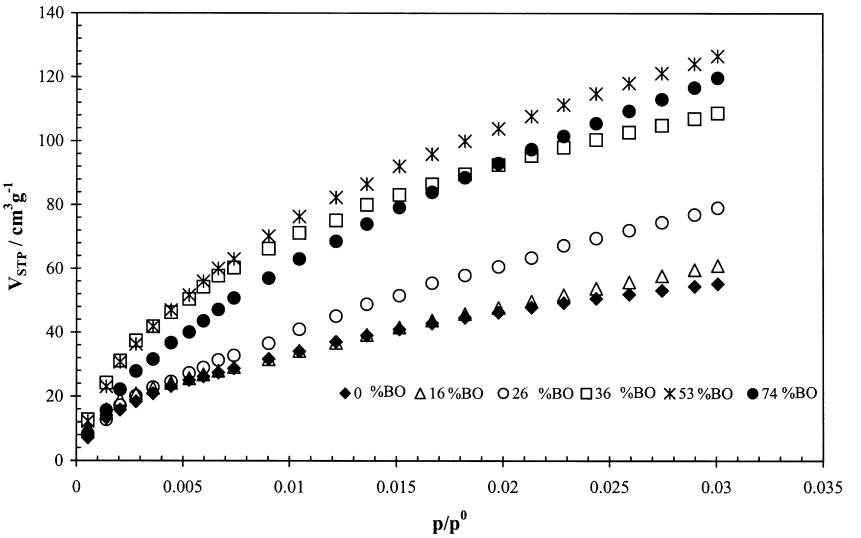

Fig. 4. Adsorption isotherms of CO_2 at 273 K on ACFs prepared by pyrolysis at 1173 K and activation at 1123 K.

and increases subsequently with the degree of BO in CO_2.

3.3. X-ray diffraction (XRD)

Chars obtained from the pyrolysis–gasification process can be crystallographically characterised by means of XRD. The height of the crystal or layer of graphitic planes L_c, its width L_a and the interplanar spacing d_{002} of the graphitic diffractions obtained for the different degrees of BO are shown in Table 3. The values obtained for d_{002} remain practically unchanged with temperature and the degree of activation. L_c for the material pyrolysed at 1173 K (1.4 nm) is slightly higher than that obtained at 1123 K (1.2 nm), and a

Table 2
Textural parameters deduced from CO_2 adsorption at 273 K

BO (wt%)	DRK method			
	$V_{\mu p}$ ($cm^3\ g^{-1}$)	$S_{\mu p}$ ($m^2\ g^{-1}$)	L (nm)	E_0 ($kJ\ mol^{-1}$)
Pyrolysis at 1123 K and activation at 1073 K				
0	0.19	524	0.93	27.8
5	0.21	586	0.94	27.6
7	0.20	554	1.00	26.1
10	0.25	703	1.00	25.8
17	0.25	684	0.98	26.4
48	0.29	789	1.19	21.8
57	0.40	1095	1.17	22.2
Pyrolysis at 1173 K and activation at 1123 K				
0	0.15	426	1.04	24.9
16	0.24	671	0.98	26.5
26	0.24	659	1.16	22.5
36	0.32	888	1.06	24.5
53	0.39	1072	1.12	23.3
74	0.42	1162	1.24	21.0

Table 3
Crystallographic parameters deduced from XRD

BO (wt%)	d_{002} (nm)	L_c (nm)	L_a (nm)
Pyrolysis at 1123 K and activation at 1073 K			
0	0.372	1.2	6.5
5	0.367	1.2	6.1
7	0.367	1.2	4.3
10	0.368	1.3	5.5
17	0.364	1.4	5.1
48	0.369	1.7	6.0
57	0.350	2.0	5.6
Pyrolysis at 1173 K and activation at 1123 K			
0	0.355	1.4	5.9
16	0.365	1.2	4.2
26	0.366	1.5	5.0
36	0.369	1.7	4.9
53	0.366	1.7	4.7
74	0.389	1.8	6.5

tendency to increase with the degree of activation is observed. On the contrary, it is difficult to define a tendency from the L_a values.

4. Discussion

Fig. 1 shows the relationship between BO and time, at constant gasification temperature. The gasification rates can be considered constant over the activation times studied. The rates obtained from the slopes ($0.5\ mg\ min^{-1}$ at 1073 K and $0.9\ mg\ min^{-1}$ at 1123 K) increase with temperature, in agreement with other reports [7,13,14]. These figures are lower than those obtained for gasification of Kevlar 49 [5,15] and Kevlar pulp [7] and similar to those reported for CO_2 activation of Nomex chars [15]. Tomlinson et al. [15] attributed the higher reactivity of Kevlar compared with that of Nomex to the catalytic effect of metallic residues present on the surface of the former. According to these authors, these inorganic particulate residues provide sites where localised carbon gasification causes pitting; otherwise one would have expected to find the opposite reactivity sequence on the basis of crystallinity differences. Additionally, one can consider that the lower reactivity of Nomex chars is associated with their lower S_{ext} compared with that of Kevlar chars [7].

N_2 isotherms for both pyrolysis/activation temperatures show the same shape (Type I, characteristic of a microporous material), in the whole BO range. However, N_2 adsorption isotherms obtained from Kevlar had some Type IV contribution. It can be observed, too, that the slope of the linear zone of the isotherms obtained with Nomex chars is constant [Fig. 2(a) and (b)], indicating that the external surface does not increase significantly with the degree of BO, and this can also be observed in Table 1. The external surface is lower than that found with Kevlar chars [7]. Another clear difference between the behaviour of chars obtained from the two isomers is that the uptake of N_2 increases continuously with the degree of BO for ACFs from Nomex; with Kevlar pulp the uptake of N_2 started to decrease at BOs above ca 50% [7]. Here, the desorption isotherms at low BO [i.e. BO < 16%, Fig. 2(a) and (b)] do not follow the same curve as the adsorption. The low pressure hysteresis effect is usually an indication that the micropores have sizes similar to those of the molecules of the adsorbate (N_2), and this result is not found at higher degrees of BO, probably because the pores are widened there [16].

As the data from Table 1 show, both S_{BET} and V_p increase with the degree of BO. The values obtained are equivalent for both pyrolysis/

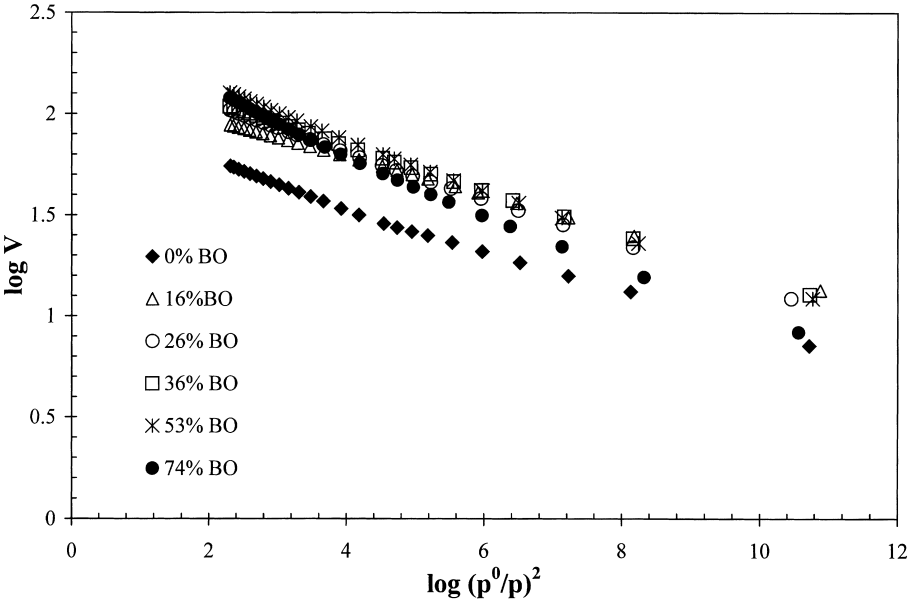

Fig. 5. DRK plots for CO_2 adsorption isotherms on ACFs prepared by pyrolysis at 1173 K and activation at 1123 K.

activation series at the same degree of BO. The external surface area S_{ext} obtained from the α_S-method does not change significantly with the degree of BO. Fig. 6 compares the evolution in some textural characteristics as a function of the degree of BO. It can be seen that the total pore volume V_p and the volume of the micropores $V_{\mu p}$ are very similar, indicating that the porosity developed is practically all microporosity. Several authors [17,18] have suggested that a subdivision

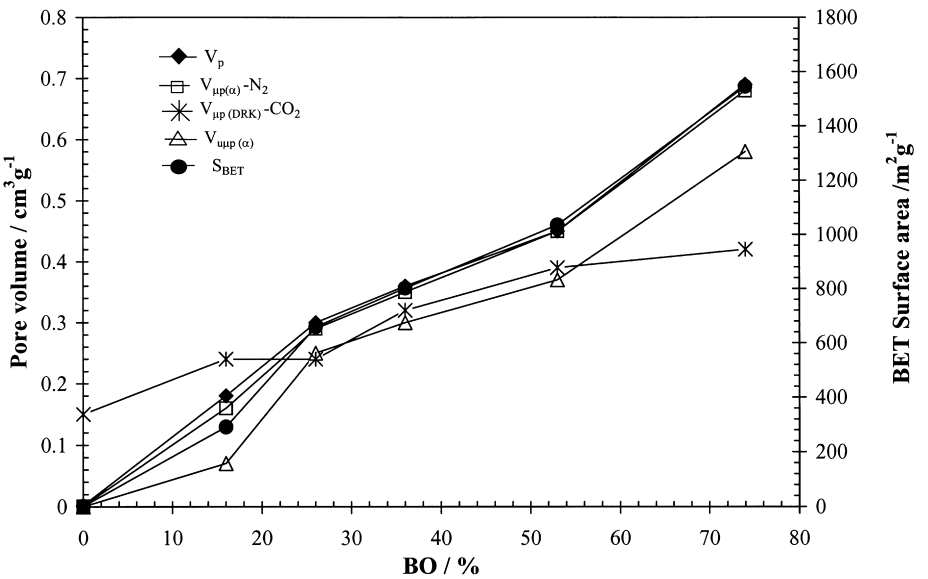

Fig. 6. Variation of several textural characteristics as a function of the BO of ACFs prepared by pyrolysis at 1173 K and activation at 1123 K.

of micropores can be made, although this is not accepted yet in the IUPAC recommendations. This division is based on different filling mechanisms: for *narrow micropores* (filled at $p/p^0 \approx 0.01$), it involves enhanced adsorbate–adsorbent interactions; for *wider micropores*, ($p/p^0 \approx 0.2$–0.3), a cooperative type of mechanism is involved. From backward extrapolation in the α_S plot (Fig. 3) the volume of the narrow micropores $V_{u\mu p}$ ($\alpha < 1$) can be calculated. The application of the α_S-method shows that $V_{\mu p}$ and the total volume of the pores V_p are very similar and, moreover, very similar to $V_{u\mu p}$ for the samples activated at intermediate BO. This indicates the creation of further narrow micropores as BO increases, and also their slight widening. At 17% of BO, practically all the porosity developed is microporosity: as Table 1 shows, 95% of the total pores are filled at $p/p^0 = 0.2$. It can be observed, too, that for the intermediate BO range (25–50%), 85–90% of that microporosity is ultramicroporosity (pores are filled up at $p/p^0 = 0.02$, Table 1). This uniform and narrow microporosity is an indication that ACFs from Nomex chars could be excellent precursor materials for the preparation of molecular sieves [19].

With the Nomex precursor used here and up to 50% BO, all the microporosity created corresponds to ultramicropores; only at BO > 50% do wider micropores start to develop. This is somewhat different than the tendency suggested previously for CO_2 activation of carbons [20]. These authors reported that, in some cases, three steps can be distinguished during the activation: up to 35% BO only small micropores (ultramicropores) are produced, and $V_{\mu p}$ remains constant; between 35 and 60% BO the volume of the medium micropores increases, but $V_{u\mu p}$ remains unchanged; finally, at BO > 60%, large micropores (supermicropores) are developed. The $V_{u\mu p}$ obtained with Nomex chars is greater than that previously found with Kevlar chars [7], this effect being more evident at BO > 50%. As indicated before, a major difference between the behaviour of the two isomers is the lower value of S_{ext} in the case of Nomex-derived chars.

Fig. 4 shows an increasing adsorption of CO_2 with the degree of BO for chars obtained from crystalline Nomex. Application of the DRK equation results in straight lines (Fig. 5), characteristic for microporous solids. The $V_{\mu p}$ results obtained from CO_2 adsorption (Table 2) are higher than those obtained from the α_S-method (N_2, 77 K) at very low BO, similar in the intermediate range of BO, and lower at higher BO (>48%, Fig. 6). At low BO, this is explained as a consequence of the easier diffusion of CO_2 at 273 K, compared with N_2 at 77 K, into the pores, which must be narrow. The lower value found for $V_{\mu p}$ at higher BO could be due to a number of factors: (i) that the pores are not so narrow and, therefore, are not filled at the low partial pressures used for CO_2 adsorption; (ii) the creation of functional groups hinders CO_2 adsorption, as observed by Parra et al. [21]. The pore width calculated from CO_2 adsorption data remains practically unchanged: the pores are slightly wider at the highest degrees of BO, and very similar for both pyrolysis/activation temperature sequences ($\sim$1 nm). This is in agreement with the slight decrease in the adsorption energy observed (Table 2).

The porosity and surface area created during activation are due to the loss of small molecules (CO and CO_2) by gasification of non-graphitic carbon and heteroatoms, the reaction with graphitic carbon and the reorganisation of layers of pseudographitic planes [22,23]. It can be observed in Table 3 that L_c shows a tendency to increase as the degree of activation increases. The L_c values amount to nearly one-half of the values found for ACFs prepared from Kevlar flock under similar conditions [8], indicating that the latter are more ordered. No significant conclusions could be drawn from either d_{002} or L_a. The interlayer d-spacing does not change significantly ($\sim$0.37 nm), and it is difficult to deduce a tendency from the L_a values due to the lack of precision in these measurements (XRD peaks in these highly disorganised carbons are very weak). Therefore, the increase of the micropore volume observed seems to be related, at a microscopic level, to an increase in the thickness of the layers of graphitic planes remaining in the activated material. This would be due to a selective gasification of the less ordered (and therefore more reactive) fractions of the carbonaceous material, whose elimination generates new micropores by reaction with the activating agent.

5. Conclusions

ACFs with a narrow pore size distribution ($\sim$1 nm) can be prepared by pyrolysis and CO_2 gasification of crystalline Nomex chars. As with Kevlar chars, the microstructure developed depends on the degree of BO, and not on the pyrolysis/activation temperature. Nomex-pyrolysis-derived chars appear to be less reactive that those obtained from Kevlar. The main advantage of the former is that the microporosity developed is more uniform and narrow, with less participation of mesoporosity and less external surface area. The increase of microporosity with the degree of BO seems to be related to an increase of the thickness of pseudographitic layers, caused by selective gasification of the less ordered fractions.

Acknowledgements

Financial support from CICYT (grant MAT96-0430), FICYT (grant PB-MAT97-04) and fellowship support from the II Plan Regional de Investigación de Asturias is gratefully acknowledged. Thanks are given to Mr. Javier Fernández (DuPont–Asturias) for providing the Nomex sample.

References

[1] F. Rodríguez-Reinoso, in: H. Marsh, E.A. Heintz, F. Rodríguez-Reinoso (Eds.), Introduction to Carbon Technologies, Universidad de Alicante, Secretariado de Publicaciones, Alicante, 1997, p. 35.
[2] R.C. Bansal, J.-B. Donnet, F. Stoeckli, Active Carbon, Marcel Dekker, New York, 1988, p. 335.
[3] J.J. Freeman, F.G.R. Gimblett, R.A. Hayes, Z.M. Amin, K.S.W. Sing, in: F. Rodríguez-Reinoso, J. Rouquerol, K.S.W. Sing (Eds.), Characterization of Porous Solids II, Elsevier, Amsterdam, 1991, p. 319.
[4] J.J. Freeman, J.B. Tomlinson, K.S.W. Sing, C.R. Theocharis, Carbon 31 (1993) 865.
[5] J.J. Freeman, J.B. Tomlinson, K.S.W. Sing, C.R. Theocharis, Carbon 33 (1995) 795.
[6] F. Stoeckli, T.A. Centeno, A.B. Fuertes, J. Muñiz, Carbon 34 (1996) 1201.
[7] A. Martínez-Alonso, M. Jamond, M. Montes-Morán, J.M.D. Tascón, Micropor. Mater. 11 (1997) 303.
[8] A. Cuesta, A. Martínez-Alonso, J.M.D. Tascón, R.H. Bradley, Carbon 35 (1997) 967.
[9] M.E.G. Mosquera, M. Jamond, A. Martínez-Alonso, J.M.D. Tascón, Chem. Mater. 6 (1994) 1918.
[10] S.R. Brown, B.C. Ennis, Text. Res. J. 47 (1977) 62.
[11] S.R Brown, B.C. Ennis, Polym. Degrad. Stab. 4 (1982) 379.
[12] S.-H. Yoon, B-C. Kim, Y. Korai, I. Mochida, Carbon 95, 22nd Biennial Conference on Carbon, American Carbon Society, San Diego, 1995, p. 218.
[13] C. Salinas-Martínez de Lecea, M. Almela-Alarcón, A. Linares-Solano, Fuel 69 (1990) 21.
[14] T. González, M. Molina Sabio, F. Rodríguez-Reinoso, Carbon 32 (1994) 1407.
[15] J.B. Tomlinson, J.J. Freeman, K.S.W. Sing, C.R. Theocharis, Carbon 33 (1995) 789.
[16] F. Rodríguez Reinoso, J.M. Martín-Martínez, A. Linares Solano, R. Torregrosa, in: F. Rodríguez Reinoso, J. Rouquerol, K.S.W. Sing (Eds.), Characterisation of Porous Solids II, Elsevier, Amsterdam, 1991, p. 419.
[17] F. Rodríguez-Reinoso, J. Garrido, J.M. Martín-Martínez, M. Molina-Sabio, R. Torregrosa, Carbon 27 (1989) 23.
[18] P.J.M. Carrott, R.A. Roberts, K.S.W. Sing, Carbon 25 (1987) 59.
[19] Y. Kawabuchi, S. Kawano, I. Mochida, Carbon 34 (1996) 711.
[20] M.C. Mittelmeijer-Hazeleger, J.M. Martín-Martínez, Carbon 30 (1992) 695.
[21] J.B. Parra, J.C. Sousa, J.J. Pis, J.A. Pajares, R.C. Bansal, Carbon 33 (1995) 801.
[22] P.J.M. Carrott, J.J. Freeman, Carbon 29 (1991) 499.
[23] H. Marsh, in: J.L. Figueiredo, J.A. Moulijn (Eds.), Carbon and Coal Gasification, Kluwer, Dordrecht, 1986, p. 27.